Density-functional calculations for III-V nitrides using the local-density approximation and the generalized gradient approximation

C. Stampfl* and C. G. Van de Walle
Xerox Palo Alto Research Center, 3333 Coyote Hill Road, Palo Alto, California 94304
(Received 7 October 1998)

We have performed density-functional calculations for III-V nitrides using the pseudopotential plane-wave method where the *d* states of the Ga and In atoms are included as valence states. Results obtained using both the local-density approximation (LDA) and the generalized gradient approximation (GGA) for the exchange-correlation functional are compared. Bulk properties, including lattice constants, bulk moduli and derivatives, cohesive energies, and band structures are reported for AlN, GaN, and InN in zinc-blende and wurtzite structures. We also report calculations for some of the bulk phases of the constituent elements. The performance of our pseudopotentials and various convergence tests are discussed. We find that the GGA yields improved physical properties for bulk Al, N_2, and bulk AlN compared to the LDA. For GaN and InN, essentially no improvement is found: the LDA exhibits overbinding, but the GGA shows a tendency for underbinding. The degree of underbinding and the overestimate of the lattice constant as obtained within the GGA increases on going from GaN to InN. Band structures are found to be very similar within the LDA and GGA. For the III-V nitrides, the GGA therefore does not offer any significant advantages; in particular, no improvement is found with respect to the band-gap problem. [S0163-1829(99)06107-X]

I. INTRODUCTION

The group-III nitrides (AlN, GaN, InN, and their alloys) have attracted much attention in recent years due to their great potential for technological applications (see e.g., Refs. 1–5, and references therein). In the wurtzite (ground-state) structure, AlN, GaN, and InN have direct energy band gaps of 6.2, 3.4, and 1.9 eV, respectively,[3] ranging from the ultraviolet (UV) to the visible regions of the spectrum. This implies that the $Al_xGa_{1-x}InN$ alloy system can be used to fabricate optical devices operating at wavelengths ranging from red into the UV. In addition, AlN and GaN have a high melting point, a high thermal conductivity, and a large bulk modulus.[6] These properties, as well as the wide band gaps, are closely related to their strong (ionic and covalent) bonding. These materials can therefore be used for short-wavelength light-emitting diodes (LED's) laser diodes, and optical detectors, as well as for high-temperature, high-power, and high-frequency devices. Bright and highly efficient blue[7] and green[8] LEDs are already commercially available, and diode lasers have been reported, emitting in the blue-violet range initially under pulsed conditions[9] and subsequently under continuous operation.[10]

In order to help understand and control the materials and device properties, theoretical studies can be most valuable. A growing number of first-principles calculations have been performed for these materials over the past few years. Most of these calculations are based on density-functional theory employing the local-density approximation (LDA), either in an all-electron formalism or using the pseudopotential plane-wave approach. A number of studies have also been carried out using *ab initio* Hartree-Fock methods; however, these methods are much more computationally demanding than the LDA, and they significantly overestimate the band gap. It is well known that the LDA leads to an underestimate of the band gaps in semiconductors,[11,12] as well as to overbinding. An additional problem for GaN and InN is that the LDA predicts that the Ga $3d$ and In $4d$ states overlap with the N $2s$ band forming two sets of bands.[6] Recent experiments have shown, however, that the $3d$ bands of GaN lie several eV below the N $2s$ band.[13–17] The same problems may be expected for InN. This has been explained as being due to neglect in the LDA of a combination of self-interaction and final-state screening effects.[13]

Use of the generalized gradient approximation (GGA) in density-functional-theory calculations is currently receiving increasing attention as a possible improvement over the LDA. The GGA has generally been found to improve the description of total energies, ionization energies, electron affinities of atoms, atomization energies of molecules,[18–20] and properties of solids.[21–24] Improvements have also been reported for adsorption energies of adparticles on surfaces[25,26] and for reaction energies.[27,28] Furthermore, the GGA has been shown to be crucial in obtaining activation energies consistent with experiment for H_2 dissociation.[29,30] The relative stability of structural phases also appears to be better described for magnetic[31] and nonmagnetic systems.[32,33] Recent studies by Dufek and co-workers[34,35] for transition-metal oxides reported a significant improvement in the band structure when using the GGA. In an earlier publication, however, Leung, Chan, and Harmon[31] reported no significant change in the band structure between LDA and GGA results for the same materials. Thus the effect of the GGA on the band structure is still unclear.

Given the large ionicity and wide band gap of the III nitrides, it is important to investigate the effects that the GGA may have on the electronic structure, in particular, whether it would lead to an improvement in the band gap. Since the GGA affects binding energies in other systems, one may also expect a difference in defect formation ener-

gies depending on the LDA or GGA treatment; the issue of defect formation is of prime interest in the nitrides.[36,37] As a first step, we have performed a comprehensive study of the bulk materials in the present work. To our knowledge there has only been one published calculation for the group-III nitrides employing the GGA (Ref. 38): in that work only selected lattice constants were reported.

Only a few of the published calculations have gone beyond the LDA: for wurtzite and zinc-blende AlN,[39] and for wurtzite[39] and zinc-blende GaN (Refs. 39–41) using a *GW* approach, and for wurtzite and zinc-blende GaN using simple quasiparticle schemes.[42] The calculations employing the *GW* approximation to the quasiparticle self-energy showed its effects not only on the band gaps but also on the position of the N $2s$ band and the bandwidth. Quasiparticle calculations essentially overcome the underestimate of the band gap as obtained using the LDA, and yield band structures in much better agreement with experiment; they are, however, time consuming and do not, as yet, produce self-consistent total-energy values. The *GW* calculations for GaN also did not include the *d* states as valence states, but treated them as part of the pseudopotential core. For completeness we mention two other recently introduced approaches that aim to obtain an improved electronic structure of wide-band-gap semiconductors: (i) the use of self-interaction- and relaxation-corrected pseudopotentials,[43] and (ii) a scheme involving generalization of the LDA known as the ''screened exchange'' method.[38,44]

In the present study we perform density-functional-theory calculations for AlN, GaN, and InN, using the pseudopotential plane-wave method and treating the Ga and In *d* states as valence, where we employed both the LDA and GGA for the exchange-correlation functional. We report lattice constants, bulk moduli and derivatives, cohesive energies, and band structures for AlN, GaN, and InN in the zinc-blende and wurtzite structures. We also present results for some of the bulk phases of the constituent elements.

Before undertaking extensive calculations for a new system, it is mandatory to perform various tests to assess the quality of the calculations and to establish acceptable basis sets. Comprehensive information about the performance and accuracy of our pseudopotentials is provided here, including an investigation of ghost states,[45] logarithmic derivatives, and transferability.[46] We compare our results with experiment where possible, and with other first-principles calculations, where we have made an effort to collect as many as possible of the *ab initio* results.

The paper is organized as follows. In Sec. II we give a brief description of the calculational method, and in Secs. III, IV, V, and VI we report results for nitrogen (and the N_2 dimer), AlN (and bulk Al), GaN, and InN, respectively. Section VII discusses the stability of the zinc-blende and wurtzite structures, and Sec. VIII contains the conclusions.

II. CALCULATIONAL METHOD

We use density-functional-theory and the local density approximation[47] as well as the generalized gradient approximation of Perdew *et al.*[18] (PWII) for the exchange-correlation functional. The wave functions are expanded in a plane-wave basis set, and we use an optimized tight-binding initialization scheme to improve the convergence of the strong N $2p$, Ga $3d$, and In $4d$ potentials, which are included as valence states. Details of the method and program can be found in Ref. 48.

We use *ab initio* fully separable soft pseudopotentials created by the scheme of Troullier and Martins[49] in which we include the GGA in the creation of the respective pseudopotentials[50,51] as well as in the self-consistent total-energy calculations. This approach is to be distinguished from the use of LDA pseudopotentials in an otherwise self-consistent GGA total energy calculation, i.e., where the exchange-correlation energy is treated in the GGA but the pseudopotentials are not (inconsistent treatment of the GGA, see Ref. 51), or from a *post*-LDA treatment where the electronic total energy is first minimized within the LDA and then corrected perturbatively for the GGA exchange-correlation energy. In the present work the GGA is thus treated in a fully consistent way. Relativistic effects are taken into account for the Ga and In atoms using weighted spin-averaged pseudopotentials. Specific details concerning energy cutoff and **k**-point sampling for the investigated systems are described in the corresponding sections along with the results.

III. NITROGEN

Essential tests for the pseudopotential plane-wave method involve the pseudopotential itself, e.g., logarithmic derivatives, ghost states, and transferability, as well as the physical properties of the systems of interest. We tested a number of different nitrogen pseudopotentials, in particular, we varied the reference electronic configuration and the cutoff radii r_c, and considered the inclusion or absence of the $3d$ scattering channel. The LDA and GGA pseudopotentials that we decided to use were based on best agreement with experimental results for the bond length, binding energy, and vibrational frequencies of the N_2 dimer, while still requiring a manageable basis set for the total-energy calculations. These potentials were generated in the non-spin-polarized ground-state valence electronic configuration, $2s^2 2p^3$, with cutoff radii $r_c^s = r_c^p = 1.37 a_0$. In the total-energy calculations we take the $2p$ channel as local. We found that including the *d* channel, generated in the electronic configuration $2s^2 2p^3 3d^0$ or $2s^1 2p^{1.75} 3d^{0.25}$, resulted in bond lengths that were somewhat too short, and binding energies and frequencies that were too large with respect to experiment, with the latter electronic configuration yielding the largest deviations.[52] In this work we discuss mainly the GGA pseudopotentials, but we also performed analogous tests for all the LDA pseudopotentials; the quality of the results was similar in both cases.

For computational efficiency it is convenient to transform the semilocal form of the pseudopotential operator into the fully separable nonlocal form as introduced by Kleinman and Bylander.[53] Transferable pseudopotentials should closely preserve the all-electron atomic scattering properties as given by the logarithmic derivatives at some radius outside the core region over the range of valence energies relevant to chemical bonding. In the left panel of Fig. 1 we show the logarithmic derivatives of the all-electron radial wave function (solid curve) and the pseudo-wave-functions (semilocal, dashed line; separable, dot-dashed line) demonstrating the close

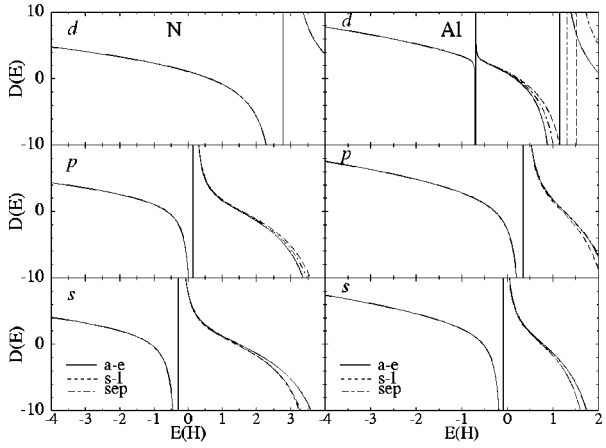

FIG. 1. Logarithmic derivatives $[d \ln R(\mathbf{r})/d\mathbf{r}$, where $R(\mathbf{r})$ is the radial wave function] vs energy E of the all-electron radial wave function (solid curve) and the (GGA) pseudo-wave-functions (semilocal, dashed line; separable, dot-dashed line) for the nitrogen atom (left panel) and the aluminum atom (right panel).

agreement of the pseudopotential and all-electron results over the relevant energy range, and the apparent absence of ''ghost states.'' When using the separable form, it is important to ensure that problems associated with ghost states are avoided. These states cannot always be easily identified by inspection of the logarithmic derivatives so we used the scheme of Gonze, Stumpf, and Scheffler[45] as implemented in the program FHIPP.[50] For all pseudopotentials discussed in the present paper, we verified that no ghost states were present. Figures 2(a) and 2(b) show, respectively, the ionic pseudopotential, and the pseudoelectron and all-electron radial wave functions. The N $2p$ potential is quite deep, resulting in the need for a large plane-wave cutoff, as we will see below. We also note that the ionic pseudopotential exhibits small short-ranged oscillations near the origin; we make no attempt to remove these, with the understanding that these oscillations are largely filtered by means of the plane-wave basis energy cutoff.[50,51]

Pseudopotentials are constructed so that they will reproduce the all-electron calculation in the reference configuration. However, the pseudopotentials should also yield accurate results in a wide range of atomic environments, i.e., they should be transferable. In order to achieve this, it is necessary that the pseudopotential reproduces the all-electron results (total energy and eigenvalues) to within the accuracy of the underlying frozen-core approximation, for different valence electron densities of the atom (e.g., excited atomic configurations) and over a desired energy range. We therefore test the transferability of the pseudopotential by monitoring the pseudo-atom ''hardness'' in a variety of electronic configurations. To do this we compare the change in energy eigenvalues and excitation (neutral charge) and ionization (positive charge) energies as a function of electron occupation as obtained using pseudopotential and all-electron calculations. In Fig. 3 we plot the *difference* of these quantities between the pseudopotential and all-electron results. In the left panel, emptying of the N $2p$ state is considered, and in the right panel excitation (or electron transfer) of electrons from the $2s$ into the $2p$ level. It can be seen that the eigenvalues and excitation energies of the pseudopotential differ increasingly from those of the all-electron potential for larger deviations from the reference electronic configuration ($2s^2 2p^3$). Given that we are considering rather large ionization and excitation energies (a maximum of 3.23 H and 0.85 H, respectively) the magnitude of the deviation is quite small, indicating good transferability for normal physical ap-

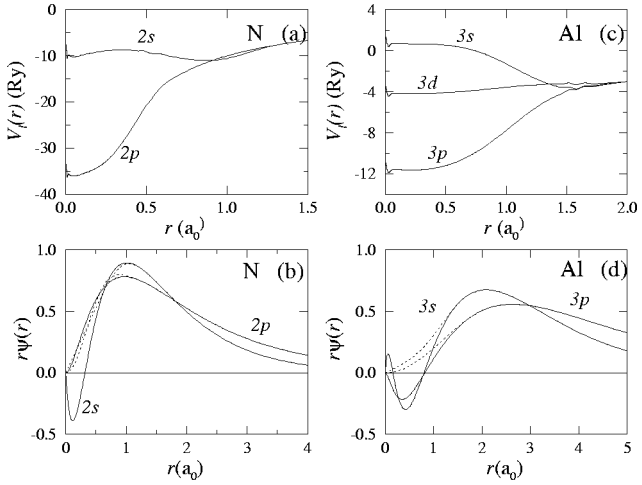

FIG. 2. Ionic GGA pseudopotential (a) and all-electron and pseudopotential (dashed line) wave function (b) for the nitrogen atom. (c) and (d) Same as (a) and (b) but for the aluminum atom.

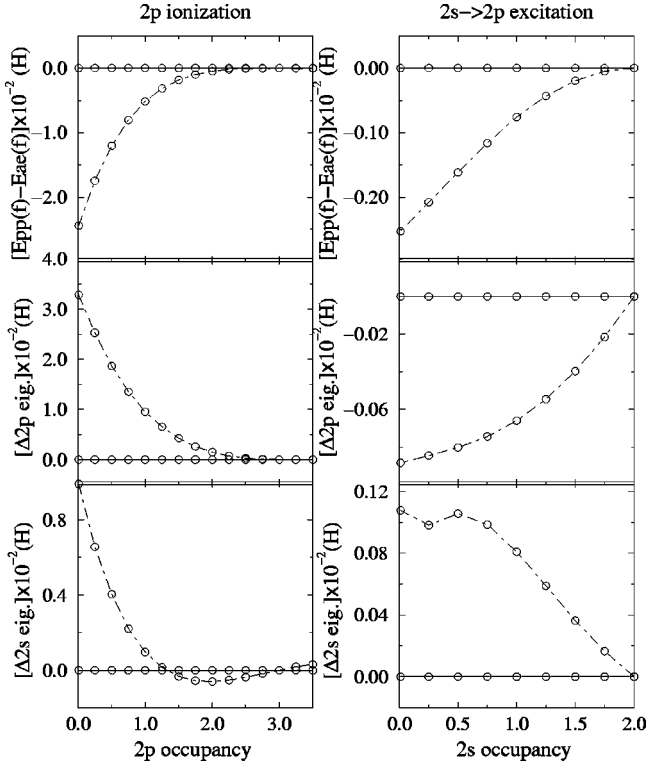

FIG. 3. Deviations in the excitation energies ($E_{\rm pp}$-$E_{\rm ae}$, where ''pp'' stands for pseudopotential and ''ae'' for all electron) and energy eigenvalues ($\Delta 2s, \Delta 2p$) of the nitrogen pseudoatom (GGA) as a function of occupation compared to all-electron results with respect to the ground-state configuration. The left panel shows results as a function of occupation of the $2p$ state (with a constant $2s$ occupation of 2 electrons) and the right panel shows results as a function of electron transfer from the $2s$ to the $2p$ state (plotted with respect to $2s$ occupation).

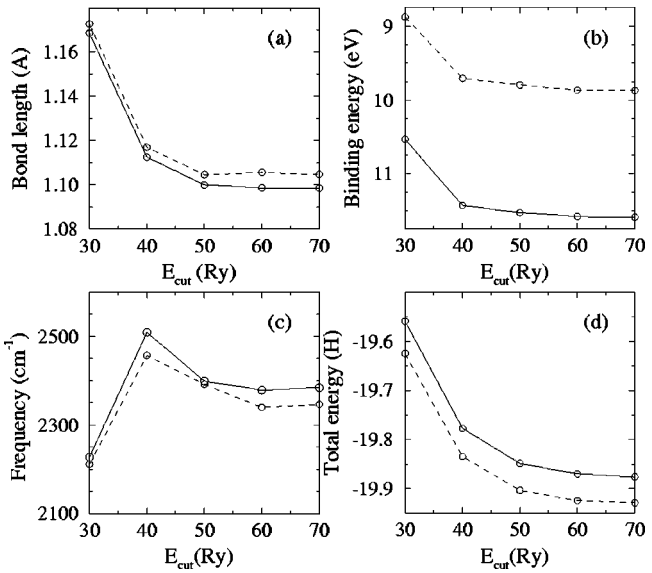

FIG. 4. Convergence of the (a) bond length, (b) binding energy, (c) frequency, and (d) total energy for N_2 as a function of cutoff energy $E_{\rm cut}$. Solid and dashed lines represent LDA and GGA results, respectively.

plications. These results can be compared, for example, to those in Refs. 46, 51, 54, and 55.

The pseudopotential should also yield accurate physical properties of the N_2 dimer. In Figs. 4(a)–4(d) we show, respectively, the calculated bond length, binding energy, vibrational frequency, and total energy as a function of the energy cutoff $E_{\rm cut}$. The equilibrium bond-length, vibrational frequency, and total energy are obtained using a third-order polynomial fit to the total energy versus N_2 bond-length curve. Corrections to the theoretical values of the binding energy for zero-point energies are not included; these are expected to be on the order of a few tenths of an eV. Zero-point energies are also not included in the cohesive energies reported in subsequent sections.

Although the absolute value of the total energy is not converged at 50 Ry, the other properties seem reasonably well converged at this cutoff. *Differences* of total energies are known to converge notably faster than the absolute energies. Even a 40-Ry cutoff yields reasonable results, but for energy cutoffs lower than 40 Ry, the results exhibit a clear lack of convergence.

Values of the calculated physical properties are listed in Table I (obtained using a 15-bohr cubic supercell and an energy cutoff of 70 Ry with the Γ-point for the **k**-space sampling). The binding energy (defined here as a positive value) is obtained as the energy difference of twice the total energy of a (spherical) N pseudoatom and the total energy of the N_2 dimer. The spin-polarization energy of the atomic ground state of the free N atom is taken into account; this energy was calculated to be 2.893 eV using the LDA and 3.151 eV using the GGA (Ref. 62); that of the free N_2 dimer is negligible. The present results agree well with previous LDA and GGA calculations. Compared to the LDA results, the GGA yields very similar, but slightly longer bond lengths, slightly lower frequencies, and significantly smaller binding energies that are closer to experiment. Similar trends have been reported for other small molecules (see, for example, Ref. 19).

TABLE I. Calculated bond length b, frequency ν, and binding energy E_b for the N_2 dimer. The particular functional used is enclosed in brackets; for the values taken from Ref. 19, the functionals are separated into exchange and correlation. The exchange part corresponds to Slater (Ref. 56) (S) or Becke (Ref. 57) (B). For correlation, either the LSD (local electron spin density) theory of Vosko, Wilk, and Nusair (Ref. 58) (VWN) or the gradient-corrected functional of Lee, Yang, and Parr (LYP) (Ref. 59) was used. PWII (Ref. 18) is the GGA employed in the present work and PWI is the earlier GGA of Perdew and Wang (Ref. 60). Present values are calculated with an energy cutoff of 70 Ry in a 15-bohr cubic supercell using one special point (Γ). Experimental values are included for comparison.

LDA calculation	b (Å)	ν ($\rm cm^{-1}$)	E_b (eV)
Present	1.099	2384	11.587
Ref. 20	1.09	2380	11.6
Ref. 19 (S-VWN)	1.111	2401	11.16
GGA calculation	b (Å)	ν ($\rm cm^{-1}$)	E_b (eV)
Present	1.105	2346	9.867
Ref. 61 (PWII)	1.104	2332	10.243
Ref. 19 (B-LYP)	1.118	2337	10.03
Ref. 20 (PWI)	1.10	2320	10.1
Ref. 20 (PWII)	1.10	2330	10.3
Expt. (taken from Ref. 20)	1.10	2360	9.9

IV. ALUMINUM NITRIDE

In this section we first discuss the performance of our Al pseudopotential and calculations for bulk Al, and then describe results for AlN in the zinc-blende and wurtzite structures.

A. Al

For the Al pseudopotential we again use the non-spin-polarized electronic ground-state configuration to create the LDA and GGA pseudopotentials, i.e., $3s^2 3p^1 3d^0$. The cutoff radii were taken to be $r_c^s = 1.80a_0$, $r_c^p = 2.10a_0$, and $r_c^d = 2.00a_0$. In the total-energy calculations the $3d$ channel is taken as local. The right panel of Fig. 1 shows the logarithmic derivatives of the all-electron radial wave function (solid curve) and the pseudo-wave-functions (semilocal, dashed line; separable, dot-dashed line) for the Al atom, again showing a close tracking to the all-electron results in the relevant energy range. At higher energies (above 0.5 H) notable deviations occur for the d channel, but this energy range is well above that of interest in the present work. In Figs. 2(c) and 2(d) we show the ionic pseudopotential, and the pseudoelectron and all-electron radial wave functions. The much softer potential of the Al atom is apparent, as reflected by the significantly faster convergence of the physical properties of bulk Al as a function of energy cutoff (see Fig. 5) as compared to that of N_2 (Fig. 4). Results of the transferability tests are collected in Table II; emptying of the valence electrons was considered here (positive ionization of the atom). The

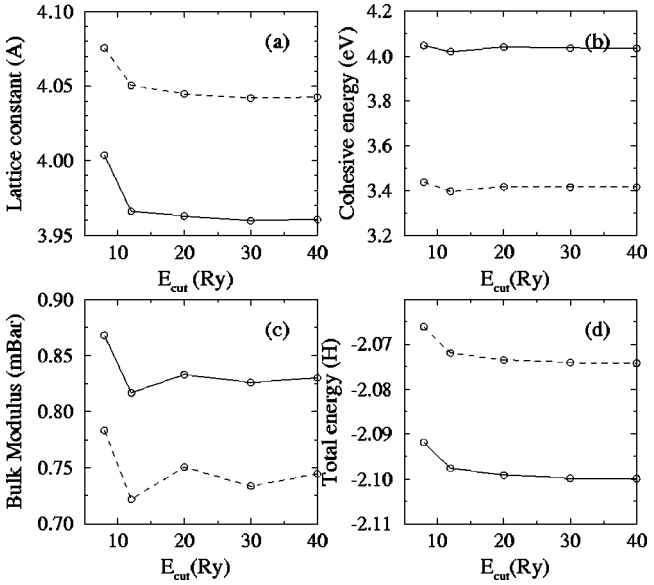

FIG. 5. Convergence of the (a) lattice constant, (b) cohesive energy, (c) bulk modulus, and (d) total energy for bulk Al as a function of cutoff energy $E_{\rm cut}$. Solid and dashed lines represent LDA and GGA results, respectively.

values in Table II are sufficiently small to indicate satisfactory transferability (see Refs. 46, 51, 54, and 55).

In Fig. 5 the convergence of the physical properties of bulk Al is tested with respect to the energy cutoff. We obtained the equilibrium geometry by computing the total energy per atom in bulk, varying the lattice constant within about $\pm 5\%$ of the equilibrium value and using the Murnaghan equation of state.[63] From these data we also derived the bulk modulus and its derivative. To calculate the cohesive energy (defined here as a positive value), we take into account the spin-polarization energy of the free Al atom which is calculated to be 0.136 eV for the LDA and 0.188 eV for the GGA.[62] At about $E_{\rm cut}=12$ Ry the system may be regarded as being satisfactorily converged, i.e., the differences in the values of the lattice constant, cohesive energy, and bulk modulus obtained at 12 and 40 Ry are -0.005 Å, 0.015 eV, and 0.014 Mbar, respectively, for the LDA, and -0.008 Å, 0.019 eV, and 0.022 Mbar, respectively, for GGA. Our results indicate that the rates of convergence of the various physical properties are very similar for the LDA and GGA.

TABLE II. Eigenvalue differences (ΔE_{3s},ΔE_{3p}) and ionization/excitation energy differences ($\Delta E_{\rm ion/exc}$) (in eV) for the aluminum atom between the pseudopotential (GGA) and all-electron calculations for various electronic configurations with respect to the ground-state configuration.

Configuration	ΔE_{3s}	ΔE_{3p}	$\Delta E_{\rm ion/exc}$
$3s^2\,3p^1$	0.00	0.00	0.00
$3s^2\,3p^{0.5}$	0.0003	−0.0005	0.0005
$3s^2\,3p^0$	−0.0002	−0.0024	−0.0054
$3s^{1.5}\,3p^0$	0.0192	0.0023	0.0055
$3s^{1.0}\,3p^0$	0.0792	0.0298	−0.0304
$3s^{0.5}\,3p^0$	0.3370	0.1997	−0.1301
$3s^{1.0}\,3p^{1.0}$	0.0295	0.0077	−0.0087

TABLE III. Lattice constant a, bulk modulus B and derivative B', and cohesive energy E_c, of bulk Al. Present values were obtained using an energy cutoff of 40 Ry and 182 **k** points. Experimental results are included for comparison.

LDA calculation	a (Å)	B (Mbar)	B'	E_c (eV)
Present	3.961	0.830	4.605	4.034
Ref. 51	3.97	0.83		4.09
Ref. 21	3.96	0.87		4.05
Ref. 22	3.93	0.877		4.14
Ref. 23	3.96	0.808		4.06
GGA calculation	a (Å)	B (Mbar)	B'	E_c (eV)
Present	4.042	0.744	4.417	3.415
Ref. 51	4.05	0.790		3.52
Ref. 21	4.04	0.79		3.09
Ref. 22	4.03	0.793		3.45
Ref. 23	4.03	0.720		3.51
Expt. (Ref. 64)	4.05	0.773		3.39

The calculated values obtained using $E_{\rm cut}=40$ Ry with 182 **k** points in the irreducible part of the Brillouin zone are collected in Table III. It can be seen that good agreement is obtained with other LDA and GGA calculations, all of which were calculated using the pseudopotential plane-wave method. Our GGA results show a 2.07% larger lattice constant, an 11.26% smaller bulk modulus, and a 0.619-eV smaller cohesive energy than our LDA results, and are in better agreement with experiment.

B. AlN

The ground-state structure of AlN is wurtzite, but AlN has also been reported to stabilize in the zinc-blende (cubic) structure (see Ref. 6 and references therein). The zinc-blende and wurtzite structures are schematically depicted in Figs. 6(a) and 6(b). For the zinc-blende structure, determination of the theoretical equilibrium geometry is straightforward since there is just one lattice constant a with two atoms per unit cell, one at $(0,0,0)$ and the other at $(\frac{1}{4},\frac{1}{4},\frac{1}{4})a$, with unit vectors $\mathbf{a}=(0,\frac{1}{2},\frac{1}{2})a$, $\mathbf{b}=(\frac{1}{2},0,\frac{1}{2})a$, and $\mathbf{c}=(\frac{1}{2},\frac{1}{2},0)a$. For wurtzite there are four atoms per hexagonal unit cell. With the unit vectors $\mathbf{a}=(\frac{1}{2},\sqrt{3}/2,0)a$, $\mathbf{b}=(\frac{1}{2},-\sqrt{3}/2,0)a$, and $\mathbf{c}=(0,0,c/a)a$, the positions of the atoms, in units of **a**, **b**,

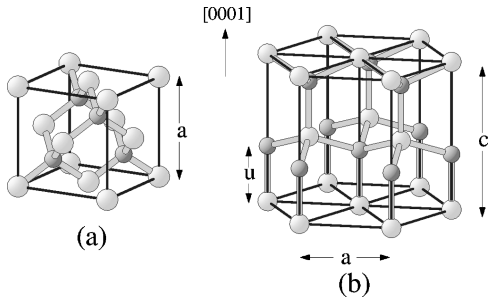

FIG. 6. Schematic illustration of (a) the zinc-blende structure and (b) the wurtzite structure. Larger and smaller spheres represent cations and anions, respectively.

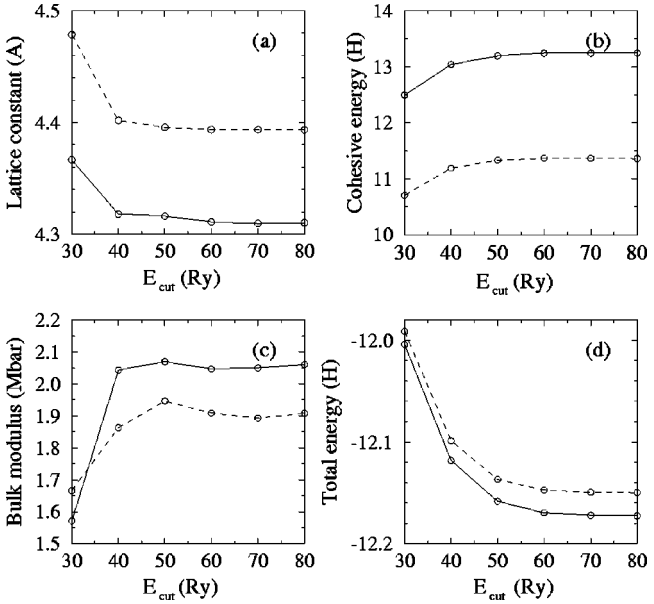

FIG. 7. Convergence of the (a) lattice constant, (b) cohesive energy, (c) bulk modulus, and (d) total energy for AlN in the zinc-blende structure as a function of cutoff energy $E_{\rm cut}$. Solid and dashed lines represent LDA and GGA results, respectively.

and **c** are (0,0,0) and $(\frac{2}{3},\frac{1}{3},\frac{1}{2})$ for atoms of the first type, and $(0,0,u)$ and $(\frac{2}{3},\frac{1}{3},u+\frac{1}{2})$ for atoms of the second type, where u is the dimensionless internal parameter. For the ideal wurtzite structure, $c/a=\sqrt{\frac{8}{3}}$ and $u=\frac{3}{8}$.

To determine the equilibrium geometry of the wurtzite phase, we optimize the independent parameters V (volume of the unit cell), c/a, and u as follows: In the first step, we assume the ideal wurtzite structure and determine the equilibrium volume by varying the lattice constant a. Then, keeping the equilibrium volume fixed and $u=\frac{3}{8}$, the c/a ratio is varied (generally in the range of 1.593 to 1.663 in steps of 0.01) to find the optimum value. At the new c/a ratio we once again vary the lattice constant a, to determine the new equilibrium volume V'. Then, having found c/a and V', we vary the internal parameter u (generally from 0.365 to 0.390 in steps of 0.005) to minimize the total energy.

To check convergence of the calculations as a function of energy cutoff $E_{\rm cut}$ we calculated the bulk properties of AlN in the zinc-blende structure as a function of $E_{\rm cut}$. The cohesive energy E_c is obtained as the difference between the total energy of the bulk material, $E_{\rm tot}^{\rm bulk}$ (per cation-anion pair), and that of the free atoms, $E_{\rm tot}^{\rm atom}$. We choose to define this energy as positive, i.e., $E_c=-E_{\rm tot}^{\rm bulk}+\Sigma_i E_{\rm tot}^{{\rm atom},i}$. The results are shown in Fig. 7. A convergence behavior similar to that of the N_2 dimer can be observed in that below 40 Ry the physical quantities are poorly converged. These results reflect the fact that the N pseudopotential is dictating the rate of convergence for AlN.

In Tables IV and V, our calculated bulk properties of AlN in the zinc-blende and wurtzite structures are presented and compared with experiment and with other published *ab initio* calculations. These results were obtained using an energy cutoff of 80 Ry with ten and 24 **k** points in the irreducible part of the Brillouin zone, for the zinc-blende and wurtzite structures, respectively. Calculations for the zinc-blende structure with 60 **k** points in the irreducible part of the Brillouin zone showed almost identical results, as was the case for GaN and InN.

TABLE IV. Lattice constant a, bulk modulus B and derivative B', cohesive energy E_c, and band gap E_g^Γ of zinc-blende AlN, calculated at the theoretical lattice constant. Methods include pseudopotential plane-wave (PPPW), pseudopotential Gaussian basis (PP-GB), all-electron (AE), and Hartree-Fock (HF). Present values were obtained using an energy cutoff of 80 Ry and 10 **k** points. Experimental results are included for comparison.

Method	LDA calculation	a (Å)	B (Mbar)	B'	E_c (eV)	E_g^Γ (eV)
PPPW	Present	4.310	2.06	3.86	13.242	4.75
	Ref. 65	4.342	2.07			4.35
	Ref. 66	4.37	2.02			4.09
	Ref. 67	4.34	2.14	3.3		
	Ref. 68	4.365				
	Ref. 69	4.421	1.95			
	Ref. 70	4.339	2.04	4.06	17.990	4.50
PP-GB	Ref. 43	4.29				
AE	Ref. 71	4.32	2.03	3.2		
	Ref. 72	4.334	2.16			
	Ref. 38	4.345	2.07			
HF	Ref. 73	4.3742	2.18		10.88	
Method	GGA calculation	a (Å)	B (Mbar)	B'	E_c (eV)	E_g^Γ (eV)
PPPW	Present	4.394	1.91	3.81	11.361	4.13
AE	Ref. 38	4.40				
Expt. (Ref. 6)		4.37				

TABLE V. Lattice constants a and c, c/a, internal parameter u, bulk modulus B and derivative B', cohesive energy E_c, and band gap E_g^Γ of wurtzite AlN, calculated at the theoretical lattice constants. Methods include pseudopotential plane-wave (PPPW), pseudopotential Gaussian basis (PP-GB), all-electron (AE), and Hartree-Fock (HF). Present values were obtained using an energy cutoff of 80 Ry and 24 **k** points. Experimental values are included for comparison.

Method	LDA calculation	a (Å)	c (Å)	c/a	u	B (Mbar)	B'	E_c (eV)	E_g^Γ (eV)
PPPW	Present	3.057	4.943	1.617	0.3802	2.09	5.58	13.286	4.74
	Ref. 65	3.084	4.948	1.604	0.3814	2.05			4.41
	Ref. 66	3.09	5.006	1.62	0.378	1.99			4.44
	Ref. 67	3.082	4.945	1.604	0.3821	2.15	3.63		
	Ref. 74	3.129	4.988	1.594	0.3825	1.95	3.74		3.09
	Ref. 75	3.110	4.979	1.601	0.382	2.02			
	Ref. 68	3.099	4.997	1.612	0.381				
	Ref. 69	3.144	5.046	1.605	0.381	1.94			
	Ref. 70	3.077	4.981	1.619	0.380	2.071	3.82	18.032	4.56
PP-GB	Ref. 43	3.05	4.89	1.603	0.382				4.2
AE	Ref. 71	3.06	4.91	1.60	0.383	2.02	3.8		
	Ref. 72 [a]	3.072	4.904	1.596	0.382	2.05			4.52
	Ref. 38	3.091	4.952	1.602	0.381	2.12			
HF	Ref. 76 [b]	3.117	4.982	1.598	0.3828	2.39	3.77	10.11	
	Ref. 76 [c]	3.101	4.975	1.604	0.3817	2.39	4.19	11.09	
	Ref. 73	3.1002	4.9888	1.6092	0.3805				
	Ref. 77	3.114	4.984	1.6005	0.3824				
Method	GGA calculation	a (Å)	c (Å)	c/a	u	B (Mbar)	B'	E_c (eV)	E_g^Γ (eV)
PPPW	Present	3.113	5.041	1.6193	0.3798	1.92	3.96	11.403	4.245
AE	Ref. 38	3.135	5.022	1.602	0.381				
	Expt. (Refs. 6, 71, and 73)	3.111	4.978	1.601	0.385	1.85–2.12	5.7–6.3	11.669	6.28

[a]This result was obtained by optimizing c/a and u, but the equilibrium volume was taken to be that of experiment.

[b]All-electron results.

[c]Pseudopotential results.

We sectioned the entries in Tables IV and V according to the calculational method for ease of comparison: pseudopotential plane-wave, pseudopotential Gaussian basis, all-electron, and Hartree-Fock methods. Table IV (zinc-blende structure) shows that the lattice constants and bulk moduli agree fairly well for all calculation methods. The largest deviation in lattice constant was reported in Ref. 69, where the obtained value was somewhat larger than the others. We note that for zinc-blende AlN the band gap is indirect; the entries in Table IV correspond to the direct band gap at Γ.

From Table V (wurtzite structure) we can see that the HF methods yield slightly larger lattice constants than the LDA results; this is a well-known effect. Table V shows no significant difference in the results of the physical properties of the all-electron and pseudopotential methods for AlN. We note that the cohesive energies obtained by Satta *et al.*[70] are significantly larger than those of the present work (by 4.748 and 4.746 eV for the zinc-blende and wurtzite structures, respectively). This is surprising since both Satta *et al.*'s and our approach takes spin-polarization of the free atoms into account. For GaN (Tables VII and VIII) and InN (Tables X and XI) the agreement is much closer (with results differing by less than 0.36 eV).

We also calculated the heat of formation ΔH_f of AlN in the zinc-blende structure at $E_{\rm cut}=80$ Ry to be -3.4 eV (LDA) and -3.0 eV (GGA). The heat of formation is calculated as $\Delta H_f = E_{\rm tot}^{\rm bulk\ AlN} - E_{\rm tot}^{\rm bulk\ Al} - 1/2 E_{\rm tot}^{\rm N_2}$ (i.e., ΔH_f is negative for a stable structure). The experimental value is -3.3 eV.[6] The absolute value of the heat of formation of the wurtzite structure will be larger by the zinc-blende/wurtzite energy difference, which we calculate to be ≈ 44 meV (see Table XII).

Our lattice constants as obtained using the GGA are about 1.95% and 1.83% larger than the LDA values, for the zinc-blende and wurtzite structures, respectively. For the zinc-blende structure the LDA result is 1.3% smaller than experiment, and the GGA result 0.55% larger. The values of the bulk moduli are also lower when calculated within the GGA: about 8% smaller than the LDA results for both the zinc-blende and wurtzite structures. The cohesive energies as obtained by the GGA are 1.881 eV (zinc blende) and 1.883 eV (wurtzite) smaller than the LDA results, largely correcting the overbinding of the LDA. The GGA values are therefore in significantly better agreement with experiment, as was the case for bulk Al and the N_2 dimer.

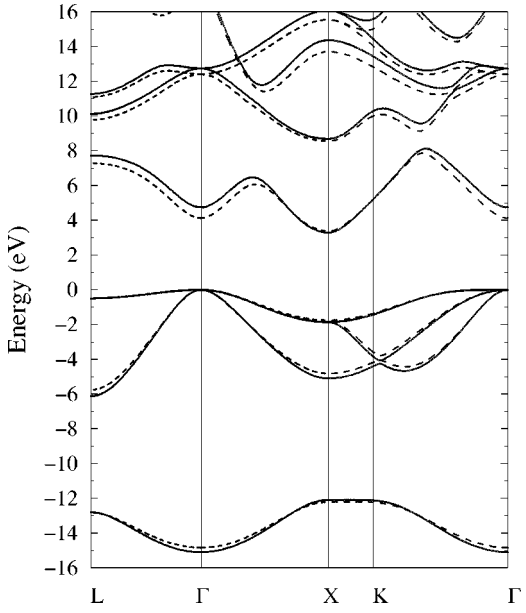

FIG. 8. Band structure of zinc-blende AlN as obtained using the LDA (solid curve) and the GGA (dashed curve), at the theoretical lattice constants appropriate for the LDA and GGA.

In Fig. 8 the band structure of AlN in the zinc-blende structure is displayed for calculations using the LDA (solid curve) and GGA (dashed curve). The band structures are calculated at the appropriate theoretical equilibrium lattice constants for the LDA and GGA, respectively. We see that the band structures are very similar, except that the band gap at Γ for the GGA result is about 0.61 eV ($\approx$13%) smaller than the LDA result. The conduction bands in the GGA calculation are shifted down slightly in energy, but the shift is not constant and depends on the **k** point and energy. Slight differences are also seen in the valence bands: in this case the GGA bands lie higher in energy than those of the LDA, leading to slightly reduced bandwidths. The differences between the LDA and GGA observed in Fig. 8 are primarily due to the larger lattice constant obtained using the GGA compared to the LDA, i.e., to deformation-potential effects. If, instead, the experimental lattice constant is used, the calculated band gap for the zinc-blende structure is the same to within 0.02 eV for the LDA and GGA.

The LDA band structure compares well with that reported in Ref. 6. The band structure for AlN in the wurtzite phase (not shown) exhibits a qualitatively similar behavior: the direct band gap for the GGA result is found to be 0.49 eV ($\approx$10%) smaller than the LDA result.

V. GALLIUM NITRIDE

As for AlN, the ground-state structure of GaN is wurtzite. Stabilization of the zinc-blende structure has been reported for growth on (001) GaAs, cubic SiC, MgO, and (001)Si (see Ref. 1 and references therein).

The LDA and GGA Ga pseudopotentials were generated in the ground-state valence electronic configuration $3d^{10}4s^24p^1$, with cutoff radii $r_c^s=2.08$, $r_c^p=2.30$, and $r_c^d=2.08$. To avoid ghost states it was necessary to take the $4s$ channel as local in the total-energy calculations. The left panel of Fig. 9 shows that the logarithmic derivatives display

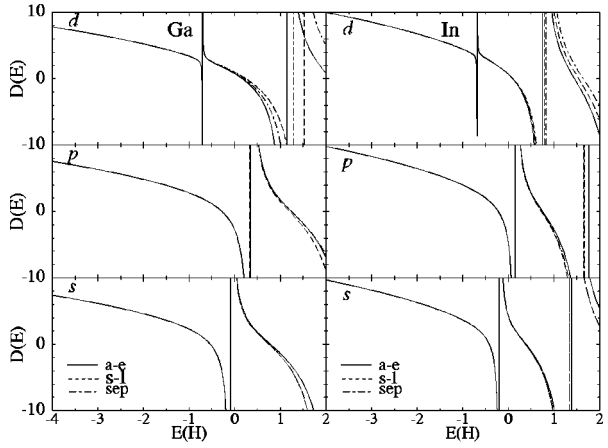

FIG. 9. Logarithmic derivatives $[d\ln R(\mathbf{r})/d\mathbf{r}$, where $R(\mathbf{r})$ is the radial wave function] vs energy E of the all-electron radial wave function (solid curve) and the (GGA) pseudo-wave-functions (semilocal, dashed line; separable, dot-dashed line) for the gallium atom (left panel) and the indium atom (right panel).

good scattering properties, as indicated by the close agreement of the all-electron and pseudopotential results in the relevant energy range. In Figs. 10(a) and 10(b) we show the ionic pseudopotential and the pseudoelectron and all-electron radial wave functions. The depth of the Ga $3d$ potential indicates that a large energy cutoff is necessary to treat the Ga $3d$ states, as we will see below.

Results of the transferability or ''hardness'' tests are collected in Table VI. Similar to our tests for the Al atom, we consider emptying of the valence states in accord with the cationic nature of Ga in GaN. We also considered two excited electronic configurations. Good transferability is observed; these values can be compared with those reported in Ref. 54 in which the transferability of a Ga pseudopotential was also considered. In that work, however, the Ga $3d$ state was included in the core. The authors of Ref. 54 found that the partial core correction scheme[79] substantially improved the transferability, while without it the transferability was not very satisfactory. A similar improvement when using the

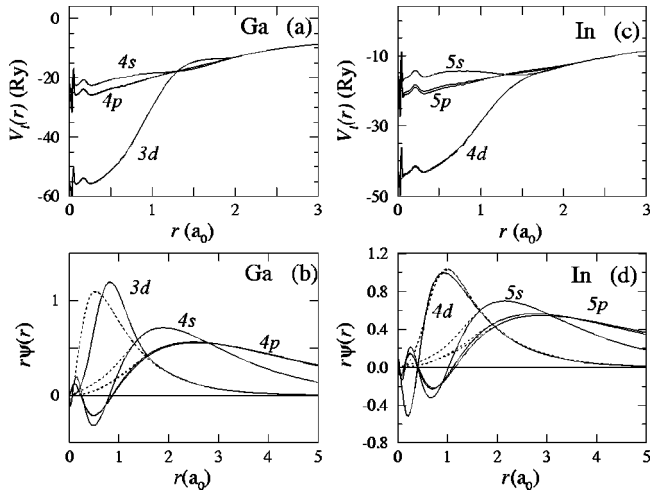

FIG. 10. Ionic GGA pseudopotential (a) and all-electron and pseudopotential (dashed line) wave function (b) for the gallium atom. (c) and (d) Same as (a) and (b) but for the indium atom.

TABLE VI. Eigenvalue differences (ΔE_{3d},ΔE_{4s},ΔE_{4p}) and ionization/excitation energy differences ($\Delta E_{\text{ion/exc}}$) for the gallium atom (in eV) between pseudopotential (GGA) and all-electron calculations for various electronic configurations with respect to the ground-state configuration.

Configuration	ΔE_{3d}	ΔE_{4s}	ΔE_{4p}	$\Delta E_{\text{ion/exc}}$
$3d^{10}4s^{2}4p^{1}$	0.00	0.00	0.00	0.00
$3d^{10}4s^{2}4p^{0.5}$	0.0090	0.0013	0.0003	0.0003
$3d^{10}4s^{2}4p^{0.0}$	0.0163	0.0024	0.0003	0.0005
$3d^{10}4s^{1.5}4p^{0}$	−0.0317	−0.0003	−0.0003	0.0008
$3d^{10}4s^{1.0}4p^{0}$	−0.1013	−0.0102	−0.0049	0.0043
$3d^{10}4s^{0.5}4p^{0}$	−0.2005	−0.0315	−0.0155	0.0158
$3d^{10}4s^{1.0}4p^{1.0}$	−0.0807	−0.0017	0.0013	0.0014
$3d^{10}4s^{1.0}4p^{2.0}$	−0.0870	−0.0022	0.0015	0.0022

partial core correction has been reported for silicon.[46] In the present work we explicitly treat the *d* states as valence states, resulting in good transferability.

For zinc-blende GaN we calculated the lattice constant, cohesive energy, bulk modulus, and total energy as a function of energy cutoff E_{cut}. Figure 11 shows that a cutoff of at least 60 Ry is required to yield satisfactory results; the values of the bulk properties obtained using a 50-Ry cutoff are still significantly different from those at 60 Ry and higher.

In Tables VII and VIII the values of the various bulk properties are listed for the zinc-blende and wurtzite structures, as obtained using an 80-Ry cutoff and ten and 24 **k** points in the irreducible part of the Brillouin zone, respectively. For calculating the cohesive energy we again take into account the spin-polarization energy of the constituent atoms. For the Ga atom the values are 0.133 eV for the LDA and 0.182 eV for the GGA.[62] We find that the lattice constant

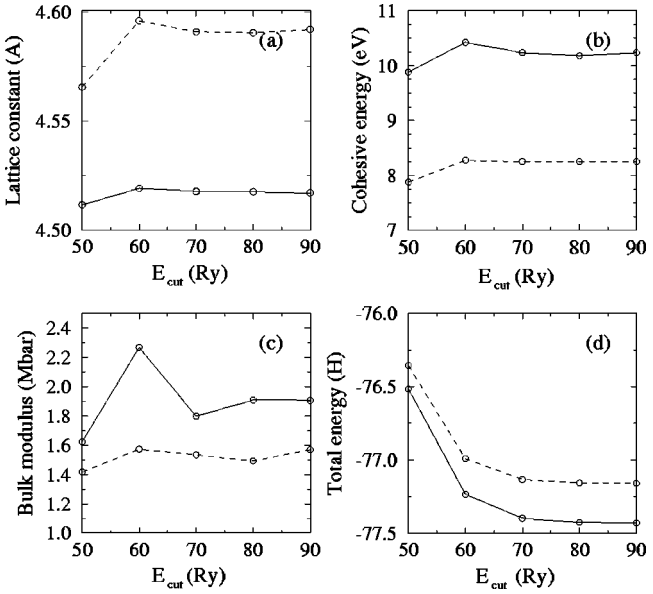

FIG. 11. Convergence of the (a) lattice constant, (b) cohesive energy, (c) bulk modulus, and (d) total energy, for GaN in the zinc-blende structure as a function of cutoff energy E_{cut}. Solid and dashed lines represent LDA and GGA results, respectively.

TABLE VII. Lattice constant *a*, bulk modulus *B* and derivative B', cohesive energy E_c, and band gap E_g^{Γ} of bulk zinc-blende GaN, calculated at the theoretical lattice constant. Methods include pseudopotential plane-wave (PPPW), pseudopotential Gaussian basis (PP-GB), all-electron (AE), and Hartree-Fock (HF). Present values were obtained using an energy cutoff of 80 Ry and 10 **k** points. Experimental values are included for comparison.

Method	LDA calculation	*a* (Å)	*B* (Mbar)	B'	E_c (eV)	E_g^{Γ} (eV)
PPPW (3*d*)	Present	4.518	1.91	4.14	10.179	1.60
	Ref. 65	4.460	1.87			1.89
	Ref. 41	4.524	2.06	3.7	10.53	
	Ref. 70	4.519	2.00	4.15	10.536	2.00
PP-GB	Ref. 43	4.45				1.60
PPPW (no 3*d*)	Ref. 66	4.51	1.92			2.15
	Ref. 68	4.364				
	Ref. 69	4.446	1.95			
	Ref. 78	4.30	2.51	2.76		
AE	Ref. 71	4.46	2.01	3.9		
	Ref. 80	4.466	1.98		10.88	2.0
	Ref. 38	4.464	1.99			
HF	Ref. 73	4.5215	2.54		8.358	
	Ref. 81	4.510	2.30	3.6		
Method	GGA calculation	*a* (Å)	*B* (Mbar)	B'	E_c (eV)	E_g^{Γ} (eV)
PPPW (3*d*)	Present	4.590	1.56	4.25	8.253	1.28
AE	Ref. 38	4.570				
Expt. (Refs. 6, 71, and 82)		4.50, 4.531	1.90			3.45,3.21

TABLE VIII. Lattice constants a, c, and c/a, internal parameter u, bulk modulus B and derivative B', cohesive energy E_c, and band gap E_g^{Γ} of bulk wurtzite GaN, calculated at the theoretical lattice constants. Methods include pseudopotential plane-wave (PPPW), pseudopotential Gaussian basis (PP-GB), all-electron (AE), and Hartree-Fock (HF). Present values were obtained using an energy cutoff of 80 Ry and 24 **k** points. Experimental values are included for comparison.

Method	LDA calculation	a (Å)	c (Å)	c/a	u	B (Mbar)	B'	E_c (eV)	E_g^{Γ} (eV)
PPPW ($3d$)	Present	3.193	5.218	1.634	0.376			10.187	1.76
	Ref. 65	3.162	5.142	1.626	0.377	2.02			2.04
	Ref. 41	3.19	5.228	1.639	0.375	2.03	4.2	10.77	
	Ref. 70	3.196	5.222	1.634	0.375	2.13	4.50	10.547	2.13
PP-GB	Ref. 43	3.15	5.13	1.628	0.372				1.70
PPPW	Ref. 66	3.2	5.216	1.63	0.376	1.91			2.29
(no $3d$)	Ref. 68	3.095	5.000	1.633	0.378				
	Ref. 74	3.126	5.119						
	Ref. 75	3.160	5.126	1.622	0.377	1.95			
	Ref. 54	3.043	4.972	1.634	0.375	2.4		8.187	3.0
	Ref. 69	3.146	5.125	1.629	0.377	1.95			
AE	Ref. 71	3.17	5.13	1.62	0.379	2.07	4.5		
	Ref. 38	3.160	5.138	1.626	0.377	1.99			
HF	Ref. 73	3.2011	5.1970	1.6235	0.3775				
	Ref. 81	3.199	5.176	1.618	0.380	2.51	2.7		
Method	GGA calculation	a (Å)	c (Å)	c/a	u	B (Mbar)	B'	E_c (eV)	E_g^{Γ} (eV)
PPPW ($3d$)	Present	3.245	5.296	1.632	0.3762	1.72	5.11	8.265	1.45
Expt. (Refs. 6, 71, 82. and 73		3.180,3.192	5.166	1.624	0.375	1.88-2.45	3.2 4.3	9.058	3.65, 3.44, 3.41

in the GGA is 1.59% and 1.63% larger than in the LDA for the zinc-blende and wurtzite structures, respectively. Correspondingly, the bulk modulus is smaller by 18% for zinc blende and 15% for wurtzite. For the zinc-blende structure we find that the LDA yields a slightly larger lattice constant than experiment (by 0.4%), while that of the GGA is 2% larger. In this case the LDA all-electron results yield lattice constants about 0.8% smaller than experiment. The cohesive energies, similarly to what we found for AlN, are also significantly smaller using the GGA as compared to the LDA: by 1.926 and 1.923 eV for the zinc-blende and wurtzite structures, respectively. The GGA cohesive energies are in slightly better agreement with experiment than the LDA values, but indicate an underbinding as opposed to the overbinding of the LDA. It appears therefore that the GGA does not bring about a significant improvement over the LDA for GaN.

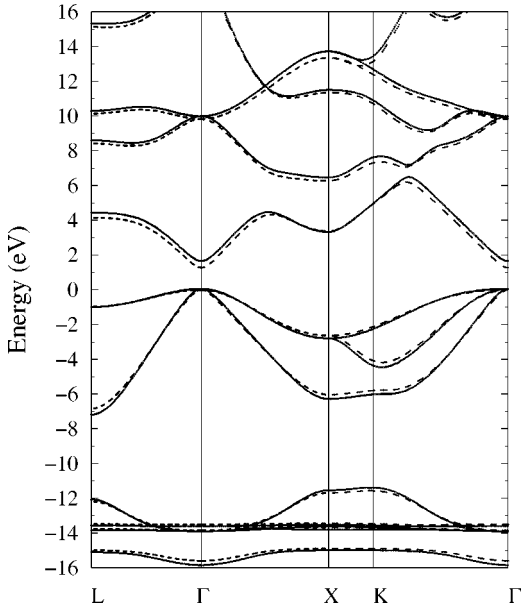

FIG. 12. Band structure of zinc-blende GaN as obtained using the LDA (solid curve) and the GGA (dashed curve), at the theoretical lattice constants appropriate for the LDA and GGA.

In Fig. 12 the zinc-blende band structure of GaN is displayed as calculated using the LDA (solid curve) and the

TABLE IX. Eigenvalue differences (ΔE_{4d},ΔE_{5s},ΔE_{5p}) and excitation energy differences ($\Delta E_{\text{ion/exc}}$) for the indium atom (in eV) between pseudopotential (GGA) and all-electron calculations for various electronic configurations with respect to the ground-state configuration.

Configuration	ΔE_{4d}	ΔE_{5s}	ΔE_{5p}	$\Delta E_{\text{ion/exc}}$
$4d^{10}5s^{2}5p^{1}$	0.00	0.00	0.00	0.00
$4d^{10}5s^{2}5p^{0.5}$	0.0142	0.0012	0.0002	0.0055
$4d^{10}5s^{2}5p^{0.0}$	0.0334	0.0024	0.0003	0.0013
$4d^{10}5s^{1.5}5p^{0}$	0.0533	0.0080	0.0024	0.0003
$4d^{10}5s^{1.0}5p^{0}$	0.0754	0.0185	0.0079	−0.0041
$4d^{10}5s^{0.5}5p^{0}$	0.0996	0.0388	0.0221	−0.0152
$4d^{10}5s^{1.0}5p^{1.0}$	0.0272	0.0091	0.0039	−0.0014
$4d^{10}5s^{1.0}5p^{2.0}$	−0.0053	0.0037	0.0016	0.0000

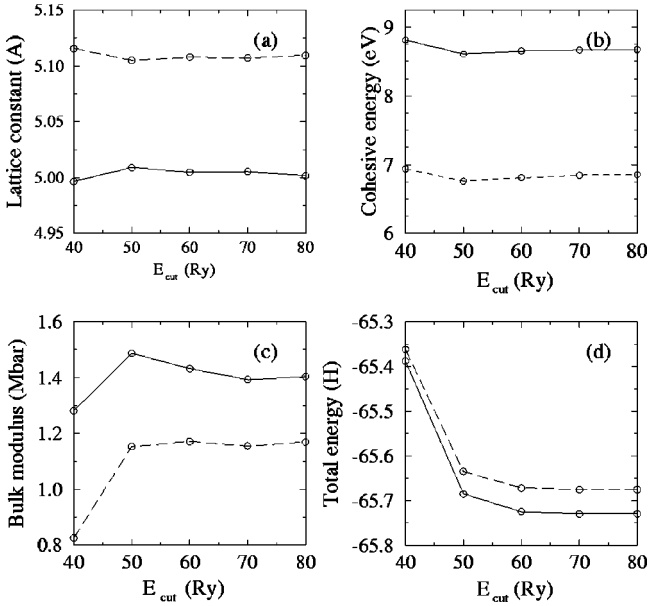

FIG. 13. Convergence of the (a) lattice constant, (b) cohesive energy, (c) bulk modulus, and (d) total energy, for InN in the zinc-blende structure as a function of cutoff energy $E_{\rm cut}$. Solid and dashed lines represent LDA and GGA results, respectively.

GGA (dashed curve), at the respective theoretical lattice constants. As in the case of AlN, the band structures look rather similar. The band gap is about 0.33 eV ($\approx$20%) smaller for the GGA as compared to the LDA. Similar results are obtained for the wurtzite structure (not shown): the GGA yields a band gap approximately 0.31 eV ($\approx$18%) smaller than the LDA. This, as mentioned earlier, can be primarily attributed to the larger GGA lattice constant.

VI. INDIUM NITRIDE

Indium nitride is perhaps the least studied of the group-III nitrides. The equilibrium crystal structure is wurtzite but the zinc-blende structure also has been reported to form.[6] Similar to the Ga pseudopotential construction, we created the LDA and GGA pseudopotentials for In assuming the ground-state valence electronic configuration $4d^{10}5s^25p^1$ with cutoff radii $r_c^s=2.08a_0$, $r_c^p=2.30a_0$, and $r_c^d=2.08a_0$. For the total-energy calculations we again find it necessary to take the s channel as local to avoid ghost states. The right panel of Fig. 9 contains the logarithmic derivatives of the GGA In potential. They appear similar to those of Ga, and display good scattering properties. In Figs. 10(c) and 10(d) we show, respectively, the ionic pseudopotential, and the pseudoelectron and all-electron radial wave functions. It can be noted that the In $4d$ potential is shallower than that of Ga $3d$ and deeper than that of N. Results of the transferability tests of the pseudopotential are given in Table IX. Again, good behavior is seen.

The convergence of lattice constant, cohesive energy, bulk modulus, and total energy as a function of cutoff energy $E_{\rm cut}$ for the zinc-blende structure is given in Fig. 13. We find that the properties of InN converge slightly faster than for GaN, but an energy cutoff of $E_{\rm cut}=50$ Ry or more is required. The values at 40 Ry cutoff are still notably different from those at 50 Ry and higher.

In Tables X and XI the structural parameters, bulk moduli and derivatives, cohesive energies, and band gaps are given for the zinc-blende and wurtzite structures as calculated in the present work and as taken from other publications. We used an 80-Ry cutoff and ten and 24 **k** points in the irreducible part of the Brillouin zone for the zinc-blende and wurtz-

TABLE X. Lattice constant a, bulk modulus B and derivative B', cohesive energy E_c, and band gap E_g^Γ of zinc-blende InN calculated at the theoretical lattice constant. Methods include pseudopotential plane-wave (PPPW), pseudopotential Gaussian basis (PP-GB), all-electron (AE), and Hartree-Fock (HF). Present values were obtained using an energy cutoff of 80 Ry and 10 **k** points. Experimental values are included for comparison.

Method	LDA calculation	a (Å)	B (Mbar)	B'	E_c (eV)	E_g^Γ (eV)
PPPW ($3d$)	Present	5.004	1.40	4.38	8.676	−0.40
	Ref. 65	4.932	1.40			−0.35
	Ref. 70	4.974	1.49	4.41	8.779	
PP-GB	Ref. 43	4.97				
PPPW (no $3d$)	Ref. 66	5.01	1.58			0.16
	Ref. 68	4.983				
AE	Feibelman (from Ref. 65)	4.953	1.44			−0.20
	Ref. 71	4.92	1.39	4.4		
	Ref. 83	4.929	1.38			
	Ref. 38	4.957	1.41			
HF	Ref. 73	4.9870	1.59		6.990	
Method	GGA calculation	a (Å)	B (Mbar)	B'	E_c (eV)	E_g^Γ (eV)
PPPW ($3d$)	Present	5.109	1.1696	4.4305	6.855	−0.55
AE	Ref. 38	5.06				
Expt. (Ref. 6)		4.98	1.37			

TABLE XI. Lattice constants a, c, and c/a, internal parameter u, bulk modulus B and derivative B', cohesive energy E_c, and band gap E_g^Γ of wurtzite InN, calculated at the theoretical lattice constants. Methods include pseudopotential plane-wave (PPPW), pseudopotential Gaussian basis (PP-GB), all-electron (AE), and Hartree-Fock (HF). Present values were obtained using an energy cutoff of 80 Ry and 24 **k** points. Experimental values are included for comparison.

Method	LDA calculation	a (Å)	c (Å)	c/a	u	B (Mbar)	B'	E_c (eV)	E_g^Γ (eV)
PPPW ($3d$)	Present	3.544	5.762	1.626	0.377	1.40	6.03	8.694	−0.27
	Ref. 65	3.501	5.669	1.619	0.3784	1.39			−0.04
	Ref. 65	3.524	5.733	1.627	0.377	1.49	4.12	8.799	
PP-GB	Ref. 43	3.53	5.72	1.620	0.378				−0.4
PPPW (no $3d$)	Ref. 66	3.55	5.787	1.63	0.375	1.62			0.16
AE	Ref. 68	3.536	5.709	1.615	0.380				
	Ref. 71	3.53	5.54	1.57	0.388	1.46	3.4		
	Ref. 38	3.528	5.684	1.611	0.380	1.41			
HF	Ref. 73	3.5428	5.7287	1.6170	0.3784				
	GGA	a (Å)	c (Å)	c/a	u	B (Mbar)	B'	E_b (eV)	E_g^Γ (eV)
PPPW ($3d$)	Present	3.614	5.884	1.628	0.377	1.161	7.33	6.872	−0.37
Expt. (Refs. 6, 71, and 73)		3.533	5.693	1.611	0.375	1.25	12.7	7.970	1.9

ite structures, respectively. We included the spin-polarization energy of the N and In atoms in obtaining the cohesive energy, where the values for the indium atom were calculated to be 0.126 eV for the LDA and 0.168 eV for the GGA.[62] The values of the (negative) band gaps at Γ, given in Tables X and XI, were obtained by evaluating the band gap as a function of lattice constant, and extrapolating to the obtained equilibrium lattice constant.

The heat of formation of InN is found to be quite small within the LDA, namely, −0.103 eV (obtained using an energy cutoff of 80 Ry). Within the GGA, the value at 80 Ry is found to be 0.394 eV (i.e., *unstable*). Reported experimental values range from −0.22 to −1.49 eV.[6] Growth of InN requires low temperatures (around 650 °C) due to the thermal instability of InN which is consistent with the calculated small values of the heat of formation.

We find that our lattice constants as obtained using the GGA are 2.10% and 1.95% larger than those obtained using the LDA for the zinc-blende and wurtzite structures, respectively. With respect to experiment, the zinc-blende LDA and GGA lattice constants are too large by 0.5% and 2.6%, respectively. The bulk moduli as obtained using the GGA are about 16% smaller for zinc blende, and 17% smaller for wurtzite. The cohesive energies, similarly to what we found for AlN and GaN, are also notably smaller for the GGA (by 1.821 eV for zinc blende and 1.822 eV for wurtzite) as compared to the LDA. We note that the LDA/GGA *differences* in cohesive energies are very similar for AlN, GaN, and InN.

In comparison with experiment we see that, as for GaN, the GGA values are somewhat too small, whereas the LDA values are too large. For InN the degree to which the GGA underbinds is larger than for GaN. Thus we find the tendency of the LDA to overbind decreases on going from GaN to InN, while the tendency of the GGA to underbind (and overestimate the lattice constant) increases on going from GaN to InN. The reason for this is at present unclear. It could be related to the pseudopotential treatment, for example, selecting the *f* channel as local and allowing a nonlocal description for each of the *s*, *p*, and *d* channels may improve the results; or it could be related to relativistic effects which increase with atomic number. In these respects, consistent, *all-electron* calculations for the cohesive energies would be informative.

In Fig. 14 the zinc-blende band structure is displayed for the LDA (solid curve) and GGA (dashed curve) calculations, at the theoretical lattice constants. In both cases InN is metallic; neither exchange-correlation functional yields a positive band gap.

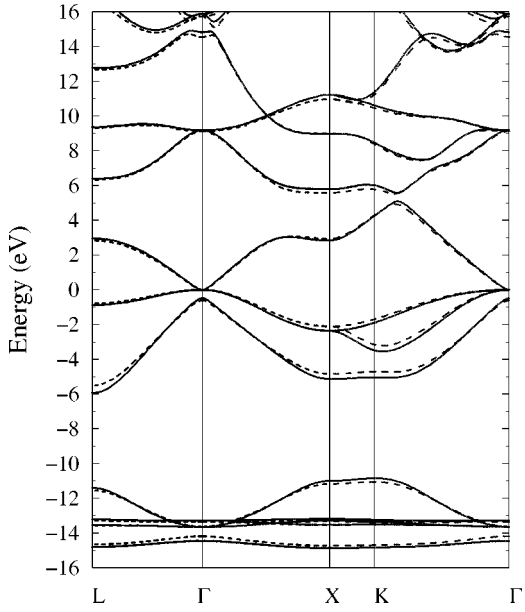

FIG. 14. Band structure of zinc-blende InN as obtained using the LDA (solid curve) and the GGA (dashed curve), at the theoretical lattice constants appropriate for the LDA and GGA.

TABLE XII. Energy difference per cation-anion pair (in meV) between the wurtzite and zinc-blende structures of the group-III nitrides. A negative value indicates the wurtzite structure is more stable.

Method	Calculation	AlN	GaN	InN
PPPW ($3d$)	Present (LDA)	−43.7	−8.4	−21.4
	Present (GGA)	−41.6	−11.6	−17.3
	Ref. 70	−42	−11	−20
PPPW (no $3d$)	Ref. 69	−37.4	−11.6	
	Ref. 68	−36.8	−19.8	−22.9
	Ref. 74		−21.2	
	Ref. 83		−30	
	Ref. 54		+17.7	
HF	Ref. 73 [a]	−97.9	−35.4	−62.6
	Ref. 73 [b]	−81.6	−27.2	−40.8
	Ref. 81		−60	
AE	Ref. 72	−86.6		
	Palummo *et al.* in Ref. 2		+70	

[a]Electron correlation energy contributions included.
[b]Electron correlation energy contributions omitted.

VII. ENERGY DIFFERENCE BETWEEN WURTZITE AND ZINC BLENDE

From the calculations described above we obtain energy differences between the wurtzite and zinc-blende structures which are given in Table XII. They are compared to results of other first-principles calculations. We find a trend of decreasing energy difference on going from AlN to InN to GaN; this trend is the same as that found in all the other studies. It can be seen, however, that there is considerable scatter in the magnitude (and in two cases, the *sign*) of the energy differences. These values are obviously quite small, and sensitive to the technical details and approximations used in the various calculation methods. In spite of this, most calculations (with the two noted exceptions) find that the wurtzite structure is the ground-state configuration and the zinc-blende structure is metastable, in accordance with experiment.

VIII. CONCLUSIONS

We have calculated various physical properties of AlN, GaN, and InN, in the zinc-blende and wurtzite structures, as well as of the N_2 dimer and bulk Al, using both the local-density approximation and the generalized gradient approximation for the exchange-correlation functional. In addition we have reported tests of our pseudopotentials and of the convergence of the total-energy calculations. For the III-V nitrides we find that using the GGA the lattice constants are 1.6–2.1 % larger, the bulk moduli 8–18 % smaller, and the cohesive energies approximately 14–20 % smaller, as compared to the LDA results. For AlN, N_2, and bulk Al, this results in a significant improvement in the physical properties obtained using the GGA. For GaN and InN, although the LDA/GGA deviations are very similar to those of AlN, the GGA does not appear to bring about any essential improvement, when compared with experiment. The GGA exhibits a tendency to underbind for these materials, which increases on going from GaN to InN. The underlying reason for this is unclear. The wurtzite/zinc-blende energy difference is found to be largest for AlN and smallest for GaN, with that of InN in between. In each case the wurtzite structure is the ground-state configuration, in agreement with experiment.

The band structures are found to be very similar in the LDA and GGA, when calculated at the experimental lattice constant. When calculated at the appropriate theoretical lattice constants, some differences are found, with a smaller band gap in the case of the GGA; this is essentially a deformation-potential effect. We conclude that for the III-V nitrides the GGA does not offer any advantage with respect to the band-gap problem.

ACKNOWLEDGMENTS

This work was supported in part by DARPA under Agreement No. MDA972-96-3-014. C.S. gratefully acknowledges support from the DFG (Deutsche Forschungsgemeinschaft), and thanks A. P. Seitsonen and M. Fuchs for the spin-polarization energy values and for stimulating discussions.

*Present address: Fritz-Haber-Institut, Abt. Theorie, Faradayweg 4–6, D-14195 Berlin, Germany.

[1] S. Strite and H. Morkoç, J. Vac. Sci. Technol. B **10**, 1237 (1992).
[2] *Wide-Band-Gap Semiconductors*, Proceedings of the Seventh Trieste Semiconductor Symposium, 1992, edited by C. G. Van de Walle (North-Holland, Amsterdam, 1993); also published as Physica B **185**, 1 (1993).
[3] H. Morkoç, S. Strite, G. B. Gao, M. E. Lin, B. Sverdlov, and M. Burns, J. Appl. Phys. **76**, 1363 (1994).
[4] F. A. Ponce and D. P. Bour, Nature (London) **386**, 351 (1997).
[5] S. Nakamura, Solid State Commun. **102**, 237 (1997).
[6] *Properties of Group-III Nitrides*, edited by J. H. Edgar, EMIS Datareviews Series (IEE, London, 1994).
[7] S. Nakamura, T. Mukai, and M. Senoh, Appl. Phys. Lett. **64**, 1687 (1994).
[8] S. Nakamura, M. Senoh, N. Iwasa, S. Nagahama, T. Yamada, and T. Makai, Jpn. J. Appl. Phys. **34**, L1332 (1995).
[9] S. Nakamura, M. Senoh, S. Nagahama, N. Iwasa, T. Yamada, T. Matsushita, H. Kiyaku, and Y. Sugimoto, Jpn. J. Appl. Phys. **35**, L74 (1996).
[10] S. Nakamura, M. Senoh, S. Nagahama, N. Iwasa, T. Yamada, T. Matsushita, H. Kiyoku, Y. Sugimoto, T. Kozaki, H. Umemoto, M. Sano, and K. Chocho, J. Cryst. Growth **189/190**, 820 (1998).
[11] J. P. Perdew and M. Levy, Phys. Rev. Lett. **51**, 1884 (1983).
[12] L. J. Sham and M. Schlüter, Phys. Rev. Lett. **51**, 1888 (1983).
[13] W. R. Lambrecht, B. Segall, S. Strite, G. Martin, A. Agarwal, H. Morkoç, and A. Rockett, Phys. Rev. B **50**, 14 155 (1994).
[14] J. Hedman and N. Martenson, Phys. Scr. **22**, 176 (1988).
[15] R. W. Hunt, L. Vanzetti, T. Castro, K. M. Chen, L. Sorba, P. I. Cohen, W. Gladfelter, J. Van Hove, A. Kahn, and A. Franciosi, Physica B **185**, 415 (1993).
[16] S. A. Ding, G. Neuhold, J. H. Weaver, P. Haeberle, K. Horn, O. Brandt, H. Yang, and K. Ploog, J. Vac. Sci. Technol. A **14**, 819 (1996).
[17] C. B. Stagarescu, L.-C. Duda, K. E. Smith, J. H. Guo, J. Nordgren, R. Singh, and T. D. Moustakas, Phys. Rev. B **54**, R17 335 (1996).

[18] J. P. Perdew, J. A. Chevay, S. H. Vosko, K. A. Jackson, M. R. Pederson, D. J. Singh, and C. Fiolhais, Phys. Rev. B **46**, 6671 (1992).
[19] B. G. Johnson, P. M. W. Gill, and J. A. Pople, J. Chem. Phys. **98**, 5612 (1993).
[20] A. D. Becke, in *The Challenge of d and f Electrons*, ACS Symposium Series No. 394, edited by D. R. Salahub and M. C. Zerne (American Chemical Society, Washington, DC, 1989), p. 165.
[21] A. Garcia, C. Elsaesser, J. Zhu, S. Louie, and M. L. Cohen, Phys. Rev. B **46**, 9829 (1992).
[22] Y.-M. Juan, E. Kaxiras, and R. G. Gordon, Phys. Rev. B **51**, 9521 (1995).
[23] A. Dal Corso, A. Pasquarello, A. Baldereschi, and R. Car, Phys. Rev. B **53**, 1180 (1996).
[24] M. Körling and J. Häglund, Phys. Rev. B **45**, 13 293 (1992).
[25] P. H. T. Philipsen, G. te Velde, and E. J. Baerands, Chem. Phys. Lett. **226**, 583 (1994).
[26] P. Hu, D. A. King, S. Crampin, M.-H. Lee, and M. C. Payne, Chem. Phys. Lett. **230**, 501 (1994).
[27] D. Porezag and M. R. Pederson, J. Chem. Phys. **102**, 9345 (1995).
[28] J. Baker, M. Muir, and J. Andzelm, J. Chem. Phys. **102**, 2063 (1995).
[29] B. Hammer, K. W. Jacobsen, and J. K. Norskov, Phys. Rev. Lett. **70**, 3971 (1993).
[30] B. Hammer, M. Scheffler, K. W. Jarcobsen, and J. K. Norskov, Phys. Rev. Lett. **73**, 1400 (1994).
[31] T. C. Leung, C. T. Chan, and B. N. Harmon, Phys. Rev. B **44**, 2923 (1991).
[32] N. Moll, M. Bockstedte, M. Fuchs, E. Pehlke, and M. Scheffler, Phys. Rev. B **52**, 2550 (1995).
[33] D. R. Hamann, Phys. Rev. Lett. **76**, 660 (1996).
[34] P. Dufek, P. Blaha, V. Sliwko, and K. Schwarz, Phys. Rev. B **49**, 10 170 (1994).
[35] P. Dufek, P. Blaha, and K. Schwarz, Phys. Rev. B **50**, 7279 (1994).
[36] J. Neugebauer and Chris G. Van de Walle, Phys. Rev. B **50**, 8067 (1994).
[37] C. Stampfl and Chris G. Van de Walle, Appl. Phys. Lett. **72**, 459 (1998).
[38] M. van Schilfgaarde, A. Sher, and A.-B. Chen, J. Cryst. Growth **178**, 8 (1997).
[39] A. Rubio, J. L. Corkill, M. L. Cohen, E. L. Shirley, and S. G. Louie, Phys. Rev. B **48**, 11 810 (1993).
[40] M. Palummo, L. Reining, R. W. Godby, C. M. Bertoni, and N. Boernsen, Europhys. Lett. **26**, 607 (1994).
[41] V. Fiorentini, A. Satta, D. Vanderbilt, S. Massidda, and F. Meloni, in *The Physics of Semiconductors*, edited by D. J. Lockwood (World Scientific, Singapore, 1995), p. 137.
[42] S. J. Jenkins, G. P. Srivastava, and J. C. Inkson, Phys. Rev. B **48**, 4388 (1993).
[43] D. Vogel, P. Krueger, and J. Pollmann, Phys. Rev. B **55**, 12 836 (1997).
[44] H. Rücker (unpublished).
[45] X. Gonze, R. Stumpf, and M. Scheffler, Phys. Rev. B **44**, 8503 (1991).
[46] M. Teter, Phys. Rev. B **48**, 5031 (1993).
[47] D. M. Ceperley and B. J. Alder, Phys. Rev. Lett. **45**, 566 (1980).
[48] M. Bockstedte, A. Kley, J. Neugebauer, and M. Scheffler, Comput. Phys. Commun. **107**, 187 (1997); and http://www.fhi-berlin.mpg.de/th/fhimd/code.html
[49] N. Troullier and J. L. Martins, Phys. Rev. B **43**, 1993 (1991).
[50] M. Fuchs and M. Scheffler, Comput. Phys. Commun. (to be published); and http://www.fhi-berlin.mpg.de/th/fhimd/code.html
[51] M. Fuchs, M. Bockstedte, E. Pehlke, and M. Scheffler, Phys. Rev. B **57**, 2134 (1998).
[52] We tested r_c values of both $r_c^s = r_c^p = 1.37$ and $r_c^s = 1.50$ and $r_c^p = 1.54$. The $2s$ and $2p$ channels were always generated in the $2s^2 2p^3$ configuration.
[53] L. Kleinman and D. M. Bylander, Phys. Rev. Lett. **48**, 1425 (1982).
[54] B. J. Min, C. T. Chan, and K. M. Ho, Phys. Rev. B **45**, 1159 (1992).
[55] J. S. Lin, A. Qteish, M. C. Payne, and V. Heine, Phys. Rev. B **47**, 4174 (1993).
[56] J. C. Slater, *Quantum Theory of Molecules and Solids. Vol. 4: The Self-Consistent Field for Molecules and Solids* (McGraw-Hill, New York, 1974).
[57] A. D. Becke, Phys. Rev. A **38**, 3098 (1988).
[58] S. H. Vosko, L. Wilk, and M. Nusair, Can. J. Phys. **58**, 1200 (1980).
[59] C. Lee, W. Yang, and R. G. Parr, Phys. Rev. B **37**, 785 (1988).
[60] J. P. Perdew and Y. Wang, Phys. Rev. B **33**, 8800 (1986).
[61] A. P. Seitsonen (private communication).
[62] A. P. Seitsonen and M. Fuchs (private communication).
[63] F. D. Murnaghan, Proc. Natl. Acad. Sci. USA **30**, 244 (1944).
[64] C. Kittel, *Introduction to Solid State Physics*, 6th ed. (Wiley, New York, 1986); *Semiconductors Physics of Group IV Elements and III-V Compounds*, edited by O. Madelung, Landolt-Börnstein, New Series, Group 3, Vol. 17, Pt. a (Springer, Berlin, 1981).
[65] A. F. Wright and J. S. Nelson, Phys. Rev. B **51**, 7866 (1995).
[66] M. Buongiorno Nardelli, K. Rapcewicz, E. L. Briggs, C. Bungaro, J.Bernholc, in *III-V Nitrides*, edited by F. A. Ponce, T. D. Moustakas, I. Akasaki, and B. A. Monemar, MRS Symposia Proceedings No. 449 (Materials Research Society, Pittsburgh, 1997), p. 893.
[67] K. Karch, F. Bechstedt, P. Pavone, and D. Strauch, Physica B **219**, 445 (1996).
[68] C.-Y. Yeh, Z. W. Lu, S. Froyen, and A. Zunger, Phys. Rev. B **46**, 10 086 (1992).
[69] K. Miwa and A. Fukumoto, Phys. Rev. B **48**, 7897 (1993).
[70] A. Satta, V. Fiorentini, A. Bosin, and F. Meloni, in *Gallium Nitride and Related Materials*, edited by R. D. Dupuis, J. A. Edmond, F. A. Ponce, and S. Nakamura, MRS Symposia Proceedings No. 395 (Materials Research Society, Pittsburgh, 1996), p. 515.
[71] K. Kim, W. R. Lambrecht, and B. Segall, Phys. Rev. B **53**, 16 310 (1996).
[72] N. E. Christensen and I. Gorczyca, Phys. Rev. B **47**, 4307 (1993).
[73] B. Paulus, F.-H. Shi, and H. Stoll, J. Phys. Condens. Matter **9**, 2745 (1997).
[74] P. E. Van Camp, V. E. Van Doren, and J. T. Devreese, Solid State Commun. **81**, 23 (1992); Phys. Rev. B **44**, 9056 (1991).
[75] J. L. Corkill, A. Rubio, and M. L. Cohen, J. Phys.: Condens. Matter **6**, 963 (1994).
[76] E. Ruiz, S. Alvarez, and P. Alemany, Phys. Rev. B **49**, 7115 (1994).
[77] T. Kamiya, Jpn. J. Appl. Phys. **35**, 4421 (1996).
[78] S. J. Jenkins, G. P. Srivastava, and J. C. Inkson, J. Phys. C **6**, 8781 (1994).
[79] S. G. Louie, S. Froyen, and M. L. Cohen, Phys. Rev. B **26**, 1738 (1982).

[80] V. Fiorentini, M. Methfessel, and M. Scheffler, Phys. Rev. B **47**, 13 353 (1993).
[81] R. Pandey, J. E. Jaffe, and N. M. Harrison, J. Phys. Chem. Solids **55**, 1357 (1994).
[82] R. C. Powell, N.-E. Lee, Y.-W. Kim, and J. E. Greene, J. Appl. Phys. **73**, 189 (1993); R. C. Powell, G. A. Tomasch, Y.-W. Kim, J. A. Thornton, and J. E. Greene, in *Diamond, Silicon Carbide and Related Wide Band Gap Semiconductors*, edited by J. T. Glass, R. Messier, and N. Fujimori, MRS Symposia Proceedings No. 162 (Materials Research Society, Pittsburgh, 1990), p. 525.
[83] A. Munoz and K. Kunc, Phys. Rev. B **44**, 10 372 (1991); J. Phys.: Condens. Matter **5**, 6015 (1993).